Preparation of Y-Ba-Cu-O and CeO2 Films by Laser Chemical Vapor Deposition and Their Microstructures

	ザオ ペイ
氏　　名	趙 培
授 与 学 位	博士（工学）
学位授与年月日	平成２３年９月１４日
学位授与の根拠法規	学位規則第４条第１項
研究科，専攻の名称	東北大学大学院工学研究科（博士課程）材料システム工学専攻
学 位 論 文 題 目	Preparation of Y-Ba-Cu-O and CeO_2 Films by Laser Chemical Vapor Deposition and Their Microstructures（レーザー化学気相析出法による Y-Ba-Cu-O および CeO_2 膜の合成とその微細構造）
指 導 教 員	東北大学教授　後藤　孝
論 文 審 査 委 員	主査　東北大学教授　後藤　孝
	東北大学教授　山根　久典
	東北大学教授　増本　博

Outline of the thesis

Chapter 1 Introduction

In this chapter, the discovery history of $YBa_2Cu_3O_{7-\delta}$ (YBCO) and CeO_2 materials were introduced. The first superconducting material was discovered at the end of the 19th century. In the following years, several key steps were spanned. The first key step in understanding superconductivity occurred in 1933, when Meissner and Ochsenfeld discovered that superconductors expelled applied magnetic fields. The second key step was on the understanding of mechanism of superconducting phenomena, which was known as the BCS theory proposed by Bardeen, Cooper, and Schrieffer. The following breakthrough in superconducting field was made in 1986. A Lanthanum, Barium, Copper and oxygen ceramic compound (La-Ba-Cu-O) with a T_C of 30 K was synthesized. Sparked by this discovery, Jing Wu Zhu research team achieved an exciting T_C of 93 K in Y-Ba-Cu-O ceramics. For the first time a material had been found that would maintain zero resistance in liquid nitrogen (77 K).

Chapter 2 Preliminary investigation

In this chapter, the problems and solution on the preparation of YBCO and CeO_2 films for present status were expatiated. In practical application, the manufacture of superconducting power cable, generators, scanners and so on require flexible superconducting wire with a long length up to sever kilometers. In order to meet this requirement, the Hastelly C276 tape is employed as the substrate. The Hastelloy C276 tape is random and has no in-plane aligned grains. However, highly in-plane aligned grains for YBCO film are required in the practical applications. Therefore, a contradiction arises. The solution to this problem is to deposit template film of $Gd_2Zr_2O_7$ by ion beam assisted deposition (IBAD) technique. After deposition of $Gd_2Zr_2O_7$ film on random Hastelly C276 by IBAD technique, the $Gd_2Zr_2O_7$ film containing in-plane aligned grains was obtained. After this, several buffer layers of MgO, $LaMnO_3$ and CeO_2 were also deposited. The MgO, $LaMnO_3$ and CeO_2 buffer layers can prevent the oxidization of the metal substrate at high temperature, can reduce lattice mismatches and the

thermal coefficient mismatches between YBCO film and $Gd_2Zr_2O_7$ template, and can transfer cubic texture from the $Gd_2Zr_2O_7$ template to YBCO film.

Various film-preparation techniques including sol-gel, metalorganic deposition using trifluoroacetates, multilayer evaporation, thermal evaporation, pulsed laser deposition, sputtering molecular beam deposition and metalorganic chemical vapor deposition (MOCVD) has been developed for preparation of YBCO and CeO_2 films. The main problem for the above preparation techniques is the relatively low deposition rate. In practical application, high speed preparation of YBCO and CeO_2 films is required. Laser chemical vapor deposition (termed laser CVD) could be an effective approach to prepare high quality YBCO film and its buffer layer CeO_2 film at high deposition rate. In the present study, laser CVD was employed to prepare YBCO and CeO_2 films on different substrates including polycrystalline Al_2O_3, single crystal $LaAlO_3$, MgO $SrTiO_3$ and Hastelloy C276 tape.

Chapter 3 Preparation of YBCO films by laser CVD

This chapter depicted preparation of YBCO films on polycrystalline Al_2O_3 substrate, on (100) MgO, $LaAlO_3$ and $SrTiO_3$ single crystal substrates and on Hastelloy C276 tape by laser CVD. YBCO film on polycrystalline Al_2O_3 substrate showed a *c*-axis preferred orientation and had rectangular grains about 30 μm in size. The deposition rate of the film was up to100 μm h^{-1}. For the YBCO films on (100) MgO, $LaAlO_3$ and $SrTiO_3$ single crystal substrates, the preferred orientation changed from *a*-axis to *c*-axis with increasing laser power. The *c*-axis-oriented YBCO films showed 0° rotated epitaxial growth mode and had maximum T_C of 90 K. The deposition rate of the *c*-axis-oriented films were 57-90 μm h^{-1}. In the case of YBCO films on Hastelloy C276 tape, *a*-axis- and *c*-axis-oriented YBCO films were also obtained. The deposition rate of *c*-axis oriented YBCO films was 83 μm h^{-1}, and this is about 3–900 times higher than that of YBCO by conventional MOCVD. The diffraction pattern of the *c*-axis-oriented film has *c*-axis-oriented grains with their *c*-axis normal to the substrate surface (Fig. 1(a, b)). The resistivity of *c*-axis-oriented YBCO films decreased linearly with lowering the temperature in normal state and showed sharp zero resistance transitions at 90 K (Fig. 1(c)). The pole figure on the (102) reflection of the *a*-axis-oriented YBCO film showed a fourfold pattern at around α = 57°, which was attributed to the {102} planes with the complementary angle of 33° to the (100) plane. The {102} planes appeared twice with a repeating angle of 90°. This was attributed to the twinning structure of *a*-axis-oriented grains. The azimuth angles β of the four pole peaks from the YBCO (102) reflection rotated 45° with respect to

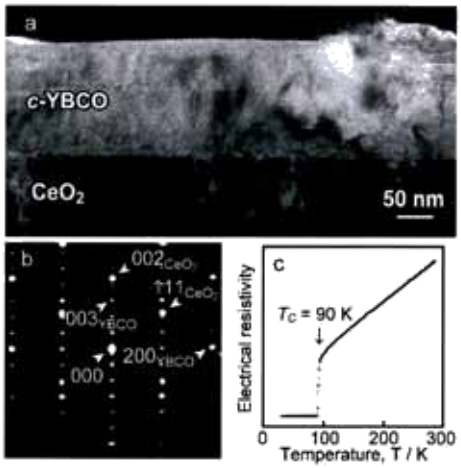

Fig. 1 TEM image (a), electron diffraction pattern (b) and electrical conductivity of a *c*-axis oriented YBCO films prepared on Hastelloy C276 tape by laser CVD.

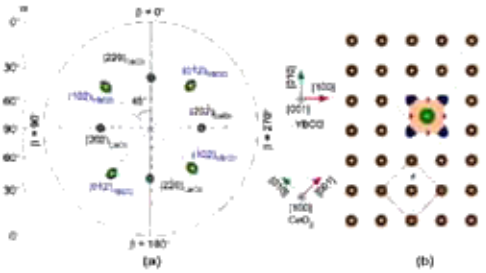

Fig. 2 Pole figure (a) and atomic arrangement relationship between YBCO film and CeO_2 film.

those of the CeO_2 (220) reflection, suggesting the YBCO [001] // CeO_2 [011] in-plane epitaxy. The pole figure diffraction pattern of the (102) reflection of the *a*-axis- and *c*-axis-cooriented YBCO film showed a strong fourfold pattern at around $\alpha = 33°$ and a weak fourfold pattern at around $\alpha = 57°$. The strong fourfold pattern came from the *c*-axis-oriented grains and was attributed to the {102} planes with the complementary angle of 57° to the (001) plane, and the weak fourfold pattern came from the *a*-axis-oriented grains and was attributed to the {102} planes with the complementary angle of 33° to the (100) plane. The weak fourfold pattern indicated the existence of twinning structure of *a*-axis-oriented grains in the present film. The azimuth angles β of the pole peaks from (102) reflection of the YBCO film rotated 45° with respect to those of CeO_2 (220) reflection, indicating the in-plane alignment growth of YBCO [001] // CeO_2 [011] for the *a*-axis-oriented grains and of YBCO [100] // CeO_2 [011] for the *c*-axis-oriented grains. The pole figure from the (102) reflection of the *c*-axis-oriented YBCO film showed a fourfold pattern at around $\alpha = 33°$, which was attributed to {102} planes with the complementary angle of 57° to the (001) plane (Fig. 2(a)). The azimuth angles β of the pole peaks from (102) reflection of the *c*-axis-oriented YBCO film rotated 45° with respect to those of CeO_2 (220) reflection (Fig. 2(a)), indicating the in-plane alignment growth of YBCO [100] // CeO_2 [011] (Fig. 2(b)).

Chapter 4 Preparation of CeO_2 films by laser CVD

In this chapter, CeO_2 films prepared on polycrystalline Al_2O_3 substrate, on *r*-cut sapphire, on (100) $SrTiO_3$ single crystal substrate and on Hastelloy C276 tape by laser CVD were studied. The (100)-oriented CeO_2 films on polycrystalline Al_2O_3 substrate had granular grains and showed a columnar cross section. The maximum deposition rate of (100)-oriented CeO_2 films was 43 μm h^{-1}. In the case of CeO_2 films on (100) $SrTiO_3$ single crystal substrate, CeO_2 films cannot form at laser power (P_L) < 52 W, with corresponding deposition temperature (T_{dep}) < 952 K. Highly (100) oriented CeO_2 films were obtained at the whole P_L from 52 to 182 W (T_{dep} = 952-1119 K). At P_L > 182 W (T_{dep} > 1119 K, the substrate began to be eroded by the laser beam. For the CeO_2 films on $SrTiO_3$, their pole figure patterns showed fourfold reflections at $\alpha = 45°$, attributing to the {220} planes. The pole figure pattern from $SrTiO_3$ (110) showed a fourfold reflection at $\alpha = 45°$, attributing to the {110} planes. The azimuth angle β of the four pole peaks from the CeO_2 film showed a 45° rotation on the basal plane of $SrTiO_3$ substrate, implying the in-plane epitaxy of CeO_2 [010] // STO [011]. For the microstructure of CeO_2 films on $SrTiO_3$, they showed rectangular grains in the surface (Fig. 3(a) and columnar grains in the cross section. Magnified surface image of CeO_2 films on $SrTiO_3$ showed two types of CeO_2 grains. One was elongated grains with trapezoidal caps whose facets attributing to {111} planes (Fig. 3). The other type was square grains with pyramid caps whose four side facets attributing to {111} planes (Fig. 3). The {111} planes had lowest surface energy (9.6 eV nm^{-2}) among the low index planes of (110), (211), (100), (210) and (310) which had surface energy of 15.3,

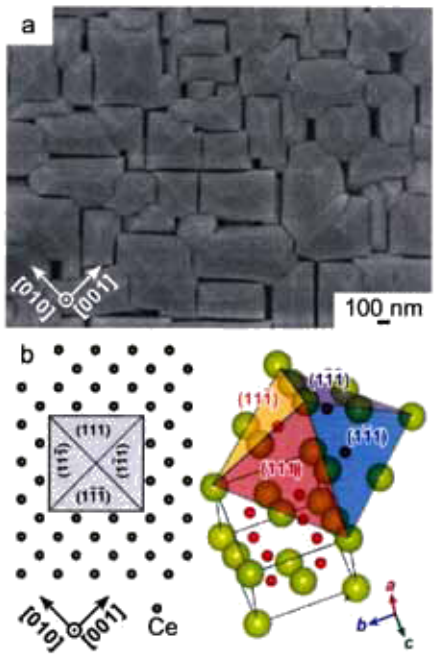

Fig. 3 Surface microstructure of CeO_2 film prepared by laser CVD and the growth mechanism on (100) $SrTiO_3$ single crystal.

16.7, 20.3, 20.4 and 22.4 eV nm^{-2}, respectively. Therefore, thus {111} planes were energetically favorable to be formed at the late deposition stage of CeO_2 film.

Single crystal CeO_2 film with a thickness of 2.5 μm was obtained at P_L = 182 W (T_{dep} = 1119 K). The cross section of the film showed dense microstructure, and no grain boundary was observed (Fig. 4(a)). The diffraction patterns from the film and substrate indicated a 45° rotated epitaxial growth relationship (Fig. 4(a, b)), which coincided with that measured by XRD pole figure. Furthermore, the film showed a smooth interface with respect to the $SrTiO_3$ substrate (Fig. 4(a)). The high resolution TEM image of the transparent CeO_2 film is shown in Fig. 4(b). No grains boundaries were observed at the whole cross section, confirming the formation of single crystal CeO_2 in the present film. From the point of mere geometric cleaving of the crystal lattice, the structure of CeO_2 along <100> direction can be decreased as a stacking of plane pairs with Ce and O atomic nets parallel to each other. This introduces a dipole moment normal to the (100) plane, leading to relatively large surface energy on (100) plane. However, the dipole moment in <100> direction could be eliminated by desorbing 50% oxygen in O atomic net at high temperature and hence the (100) plane becomes stable. Though this reconstruction, the stable (100) plane therefore could be exposed as an ending plane, as evidenced in Fig. 4.

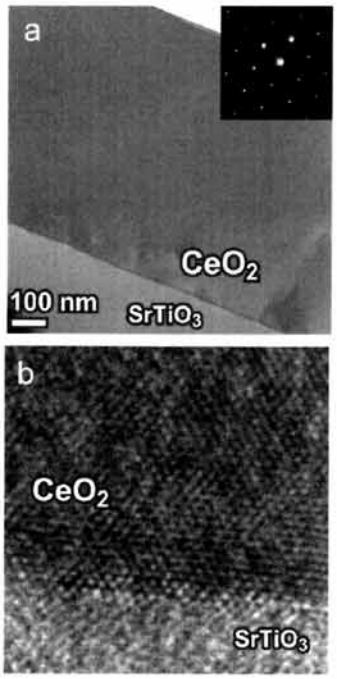

Fig. 4 TEM images of CeO_2 single-crystal film on (100) $SrTiO_3$. Inserted image shows ED pattern of the film.

Chapter 5 Summarization on the present study

High quality YBCO film was prepared on polycrystalline Al_2O_3 substrate, (100) MgO, $LaAlO_3$ and $SrTiO_3$ single crystal substrates and Hastelloy C276 tape by laser CVD. For the YBCO film on (100) MgO, $LaAlO_3$ and $SrTiO_3$ single crystal substrates, the preferred orientation changed from *a*-axis to *c*-axis with increasing P_L (T_{dep}). The *c*-axis-oriented YBCO film showed 0° rotated epitaxial growth mode and had maximum critical temperature of 90 K. The deposition rate of the *c*-axis-oriented film was 57-90 μm h^{-1}. In the case of YBCO film on Hastelloy C276 tape, a *c*-axis-oriented film with a critical temperature of 90 K was prepared at a deposition rate of 83 μmh^{-1}. The deposition rate of YBCO film obtained in the present study was 570-1000 times higher than that by MOCVD.

Highly (100)-oriented CeO_2 film was prepared on polycrystalline Al_2O_3 substrate, *r*-cut sapphire, (100) $SrTiO_3$ single crystal substrate and Hastelloy C276 by laser CVD. For the CeO_2 film on *r*-cut sapphire and (100) $SrTiO_3$ single crystal substrate, the surface of the film consisted of trapezoidal grains capped with {111} planes due to the low surface energy. The deposition rate of the film was 10-25 μmh^{-1}. In the case of CeO_2 film on Hastelloy C276, the surface of the film showed rectangular grains and cross section columnar grains. The deposition rate of the epitaxial (100)-oriented CeO_2 film had a maximum of 4.6 μmh^{-1}. The deposition rate of CeO_2 film was 50-500 times higher than that by MOCVD.

The present study demonstrated that the laser CVD is a promising technique for the preparation of YBCO film and CeO_2 film at high deposition rate.

論文審査結果の要旨

本論文は、レーザーCVD (CVD: chemical vapor deposition) 法を用いて Y-Ba-Cu-O 膜および CeO_2 膜を合成し、合成条件が膜の結晶相、配向性および微細構造に与える影響について明らかにするとともに、超電導線材合成プロセス向け Ni 基合金線材上への優れた高温超電導酸化物およびバッファ層コーティング法を開発するための指針を得ることを目的とした研究であり、全 5 章からなる。

第 1 章および第 2 章では、研究の背景を述べ、本論文の目的と構成を紹介した。

第 3 章では、Y-Ba-Cu-O 膜を様々な条件で合成し、成膜条件が膜の結晶相、配向性および微細構造に与える影響について報告した。有機金属錯体 $Y(dpm)_3$, $Ba(dpm)_2$/$Ba(tmod)_2$ および $Cu(dpm)_2$ (dpm; dipivaloylmethanate および tmod; 2,2,6,6-tetramethy1-3,5-octanedionato) を原料とし、基板予熱温度を室温から 673 K, Nd:YAG レーザー出力を 0 から 238 W、原料気化温度を 440 から 565 K、炉内圧力を 0.2 から 2 kPa の範囲内で変化させた。基板には、多結晶 Al_2O_3、(100) MgO, (100) $LaAlO_3$, (100) $SrTiO_3$ 基板を用いた。各原料気化温度を最適化することにより、多結晶 Al_2O_3 基板上であっても、高温超電導酸化物相である Y-Ba-Cu-O 膜の *c* 軸配向膜が得られた。得られた Y-Ba-Cu-O 膜は 90 K で超電導転移を示し、高温酸化物超電導体として有用であることが示された。また、成膜速度は 100 $\mu m\ h^{-1}$ に達し、レーザーCVD 法を用いることで、従来の CVD 法およびスパッタなどの気相蒸着法よりも、3-900 倍速い速度で超電導 Y-Ba-Cu-O 膜を合成できることを示した。

第 4 章では、合成温度および炉内圧力が CeO_2 膜の結晶配向成長に与える影響を調べた。基板には、多結晶 Al_2O_3、(100) $SrTiO_3$ 基板を用いた。合成温度を変化させることで、多結晶 Al_2O_3 基板上に、(100) 面に強く配向した CeO_2 膜の配向を合成することができた。 (100) $SrTiO_3$ 基板上では、面内配向した (100) CeO_2 膜がエピタキシャル成長した。(100) 配向 CeO_2 膜の微細構造を観察したところ、CeO_2 の立方晶構造を反映した {111} 面四角錐状のファセットが認められた。さらに、合成条件を最適化することで、 (100) CeO_2 単結晶膜を合成できた。

第 5 章では、本論文を総括した。

本論文により、レーザーCVD 法を用いた Y-Ba-Cu-O 膜および CeO_2 膜の合成において、合成条件と膜の結晶相、配向性および微細構造の関係を明らかにした。これらの結果は、レーザーCVD 法を用いた超電導線材合成プロセス向け Ni 基合金線材上への優れた高温超電導酸化物およびバッファ層コーティング法を開発するための指針となるものである。

よって、本論文は博士(工学)の学位論文として合格と認める。